ELSEVIER

Available online at www.sciencedirect.com

Mathematical and Computer Modelling 46 (2007) 180–188

MATHEMATICAL AND COMPUTER MODELLING

www.elsevier.com/locate/mcm

Analytical solution of nonlinear Poisson equation for symmetric double-gate metal-oxide-semiconductor field effect transistors

Shih-Ching Lo[a], Yiming Li[b,*], Shao-Ming Yu[c]

[a] *Department of Transportation Technology and Logistics Management, Chung Hua University, Hsinchu 300, Taiwan*
[b] *Department of Communication Engineering, National Chiao Tung University, Hsinchu 300, Taiwan*
[c] *Department of Computer Science, National Chiao Tung University, Hsinchu 300, Taiwan*

Received 18 May 2006; accepted 15 December 2006

Abstract

In this paper, an analytical solution of the Poisson equation for double-gate metal-semiconductor-oxide field effect transistor (MOSFET) is presented, where explicit surface potential is derived so that the whole solution is fully analytical. Based on approximations of potential distribution, our solution scheme successfully takes the effect of doping concentration in each region. It provides an accurate description for partially and fully depleted MOSFET devices in different regions of operation. Comparison with numerical data shows that the solution gives good approximations of potential for MOSFETs under different biases and geometry configurations. The solution can be applied to estimate classical and quantum electron density of nanoscale double-gate MOSFETs.
© 2007 Elsevier Ltd. All rights reserved.

Keywords: Analytical solution; Poisson equation; Surface potential; Double-gate MOSFET

1. Introduction

Advanced integrated circuit (IC) technology imposes new challenges for semiconductor devices [1–13]. Nowadays, double-gate metal-oxide-semiconductor field effect transistors (DG-MOSFET) have attracted much attention due to their improved physical properties compared with the single-gate MOSFETs [1–4,9,12]. One of the important questions is how to analytically calculate the characteristics of a device in an efficient and accurate way, especially for large scale IC simulation. Among the characteristics of a device, the potential dominates the main mechanism of operation of a device. As the potential is obtained, carrier density and transport current can be derived accordingly. Unfortunately, many solution approaches to the nonlinear Poisson equation were based on very strong assumptions and simplifications; therefore, they cannot be applied to simulate DG-MOSFET circuits accurately [3–5].

Therefore, the purpose of this work is to introduce a new one-dimensional (1-D) closed-form analytical approximation of potential distribution in the silicon film of a DG-MOSFET in different regions of operation, such as the depletion, the weak inversion, and the strong inversion. The solution is derived based on the physical mechanism

* Corresponding address: P.O. BOX 25-178, Hsinchu 300, Taiwan.
E-mail address: ymli@faculty.nctu.edu.tw (Y. Li).

0895-7177/$ - see front matter © 2007 Elsevier Ltd. All rights reserved.
doi:10.1016/j.mcm.2006.12.018

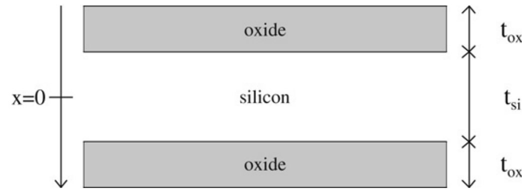

Fig. 1. An illustration of the examined DG-MOSFET.

in each region. To make the solution be a fully analytical one, the explicit form of surface potential is also derived by integrating the continuous condition. A comparison with numerical data shows that the solution gives an accurate approximation of potential distribution for a nanoscale DG-MOSFET in all regions of operation. The analytical potential can be incorporated into a quantum correction formula to account for the quantum mechanical effect on the electron density.

The remaining content of this paper is as follows. In Section 2, the nonlinear Poisson equation is presented firstly and an analytical solution is derived under several cases and approximations. Also, the explicit equation of surface potential is derived in this section. Computational concerns are given in Section 3, where results of analytical solution are compared with the numerical results. The analytical potential is further incorporated into a quantum correction formula to explore the quantum mechanical effect on the electron density in Section 4. Section 5 draws the conclusions.

2. The nonlinear Poisson equation and analytical solution

The investigated 1-D symmetric DG-MOSFET is illustrated in Fig. 1. The Poisson equation governs the operation of semiconductor devices. It comes from Maxwell's first equation, which in turn is based on Coulomb's law for electrostatic force of a charge distribution. The Poisson equation is given as

$$\Delta\phi = -q\left(p - n + N_d - N_a\right)/\epsilon_{\text{si}}, \tag{1}$$

where Δ is the Laplace operator, ϕ is potential, ϵ_{si} is dielectric constant of silicon, q is electron charge, $p(x)$ is density of hole, $n(x)$ is density of electron, N_a is doping concentration of acceptor impurity and N_d is doping concentration of donor impurity. In the silicon, $p(x) = N_a$ and $n(x) = \left(n_i^2/N_a\right)$, where n_i is intrinsic concentration. With the Boltzmann relationship, we have $p(x) = N_a \exp(-q\phi/V_t)$ and $n(x) = \left(n_i^2/N_a\right)\exp(q\phi/V_t)$, where V_t is thermal voltage, which is considered as a constant. Therefore, the Poisson equation and the boundary conditions can be rewritten as

$$\begin{cases} \Delta\phi = \dfrac{qN_a}{\epsilon_{\text{si}}}\left[1 - \exp\left(-\dfrac{\phi}{V_t}\right) + \left(\dfrac{n_i}{N_a}\right)^2\left(\exp\left(\dfrac{\phi}{V_t}\right) - 1\right)\right], & \dfrac{-t_{\text{si}}}{2} < x < \dfrac{t_{\text{si}}}{2} \\ \phi = \phi_s, \quad \partial\phi/\phi x = -C_{\text{ox}}\left(V_G - V_{\text{FB}} - \phi_s\right)/\epsilon_{\text{si}}, \quad x = \dfrac{-t_{\text{si}}}{2} \\ \phi = \phi_s, \quad \partial\phi/\phi x = C_{\text{ox}}\left(V_G - V_{\text{FB}} - \phi_s\right)/\epsilon_{\text{si}}, \quad x = \dfrac{t_{\text{si}}}{2}, \end{cases} \tag{2}$$

where ϕ_s is surface potential. V_G is gate voltage and V_{FB} is flat-band voltage. t_{ox} is thickness of oxide, t_{si} is thickness of silicon film and C_{ox} is capacitance of oxide. Since the device is symmetric, the problem is rewritten as

$$\begin{cases} \Delta\phi = \dfrac{qN_a}{\epsilon_{\text{si}}}\left[1 - \exp\left(-\dfrac{\phi}{V_t}\right) + \left(\dfrac{n_i}{N_a}\right)^2\left(\exp\left(\dfrac{\phi}{V_t}\right) - 1\right)\right], & \dfrac{-t_{\text{si}}}{2} < x < 0 \\ \phi = \phi_s, \quad \partial\phi/\phi x = -C_{\text{ox}}\left(V_G - V_{\text{FB}} - \phi_s\right)/\epsilon_{\text{si}}, \quad x = \dfrac{-t_{\text{si}}}{2} \\ \phi = \phi_b, \quad \partial\phi/\phi x = 0, \quad x = 0, \end{cases} \tag{3}$$

where $\partial\phi/\partial x = 0$ at $x = 0$ is obtained from the assumption of symmetric applied bias [4] and ϕ_b is potential at the center of the silicon region, i.e., $\phi(x = 0) = \phi_b$. As Eq. (3) is solved, the solution of the remaining part $\left(x = 0 \text{ to } t_{\text{si}/2}\right)$ is also obtained by the symmetric property.

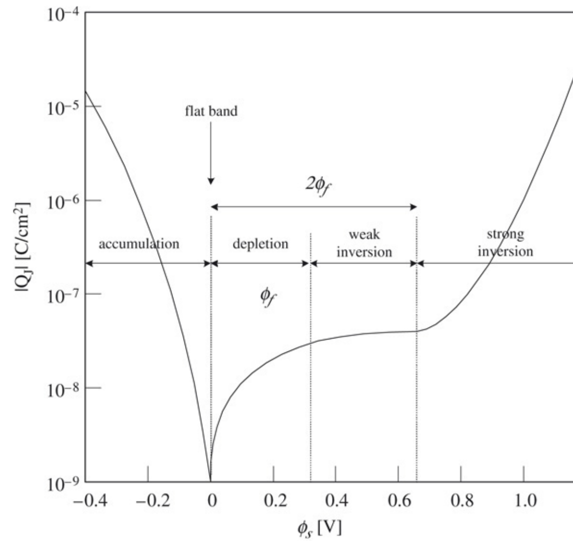

Fig. 2. Variation of total charge density in silicon as a function of surface potential ϕ_s for a MOS device.

2.1. Solution of Poisson equation

Multiplying $(\partial\phi/\partial x)\,\mathrm{d}x$ on both sides of the Poisson equation of Eq. (3) and integrating from the surface toward the center of the silicon film, i.e., $x = -t_{\mathrm{si}/2}$ to 0, we have

$$\frac{\partial\phi}{\partial x} = \pm\left\{\frac{2qN_a}{\epsilon_{\mathrm{si}}}\left\{\left[\phi - \phi_b + V_t \exp\left(\frac{-\phi_b}{V_t}\right) - V_t \exp\left(\frac{-\phi}{V_t}\right)\right] + \left(\frac{n_i}{N_a}\right)^2\left[\phi_b - \phi + V_t \exp\left(\frac{\phi}{V_t}\right) - V_t \exp\left(\frac{\phi_b}{V_t}\right)\right]\right\}\right\}^{1/2}. \tag{4}$$

Eq. (4) is a nonlinear equation, which involves polynomial and exponential functions. It needs to be simplified so as to derive its solution. According to the operating property of semiconductor devices, the solution can be discussed in two regions: (a) depletion and weak inversion region and (b) strong inversion region, which are illustrated in Fig. 2.

Let $\phi_f = V_t \ln(N_a/n_i)$. For the case of the depletion and weak inversion, we assume $0 < \phi < 2\phi_f$ and $\phi \gg V_t$, i.e., $V_t \exp(-\phi_b/V_t) - V_t \exp(-\phi/V_t) \approx 0$ and $\exp\left(\left(\phi - 2\phi_f\right)/V_t\right) - \exp\left(\left(\phi_b - 2\phi_f\right)/V_t\right) \approx 0$. Eq. (2) can be approximated and rewritten as follows

$$\frac{\partial\phi}{\partial x} = \pm\sqrt{\frac{2qN_a}{\epsilon_{\mathrm{si}}}(\phi - \phi_b)\left[1 - \left(\frac{n_i}{N_a}\right)^2\right]}. \tag{5}$$

The positive sign is for $0 < x < t_{\mathrm{si}/2}$ and the negative sign is for $-t_{\mathrm{si}/2} < x < 0$. Then, another integration of Eq. (5) yields

$$\phi = \phi_b + (\phi_s - \phi_b)\left[1 - \sqrt{\frac{qN_a}{2(\phi_s - \phi_b)\epsilon_{\mathrm{si}}}\left[1 - \left(\frac{n_i}{N_a}\right)^2\right]}\left(x + \frac{t_{\mathrm{si}}}{2}\right)\right]^2, \tag{6}$$

for $-t_{\mathrm{si}/2} < x < 0$ and

$$\phi = \phi_b + (\phi_s - \phi_b)\left[1 + \sqrt{\frac{qN_a}{2(\phi_s - \phi_b)\epsilon_{\mathrm{si}}}\left[1 - \left(\frac{n_i}{N_a}\right)^2\right]}\left(x - \frac{t_{\mathrm{si}}}{2}\right)\right]^2, \tag{7}$$

for $0 < x < t_{\mathrm{si}/2}$. Next, for the case of the strong inversion, we assume $0 < V_t \ll \phi - 2\phi_f$, i.e., $V_t \exp(-\phi_b/V_t) - V_t \exp(-\phi/V_t) \approx 0$, $\exp(\phi/V_t) - \exp(\phi_b/V_t) \gg \phi_b - \phi$ and $\exp\left((\phi - 2\phi_f)/V_t\right) - \exp\left((\phi_b - 2\phi_f)/V_t\right) \gg \phi - \phi_b$. Eq. (4) can be approximated and rewritten as follows

$$\frac{\partial \phi}{\partial x} = \pm\sqrt{\frac{2qN_a}{\epsilon_{\mathrm{si}}}\left(\frac{n_i}{N_a}\right)^2\left[V_t \exp\left(\frac{\phi}{V_t}\right) - V_t \exp\left(\frac{\phi_b}{V_t}\right)\right]}. \tag{8}$$

Also, the positive sign is for $0 < x < t_{\mathrm{si}/2}$ and the negative sign is for $-t_{\mathrm{si}/2} < x < 0$. Then, another integration of Eq. (8) gives

$$\phi = \phi_b - V_t \ln\left[\cos\left(\sqrt{\frac{qn_i^2}{2V_t\epsilon_{\mathrm{si}}N_a}}\exp\left(\frac{\phi_b}{2V_t}\right)x\right)^2\right], \tag{9}$$

for $-t_{\mathrm{si}/2} < x < t_{\mathrm{si}/2}$. Eqs. (6), (7) and (9) give the general solution of potential under weak inversion and strong inversion, respectively. However, the surface potential is still unknown. To obtain a completely analytical solution of the Poisson equation, the explicit function of surface potential is needed.

2.2. Explicit expression of surface potential

Derivation of surface potential (ϕ_s) is just the same as it is for the potential (ϕ). Firstly, multiplying $(\partial\phi/\partial x)\,\mathrm{d}x$ on both sides of the Poisson equation of Eq. (3) from the surface toward the center of the silicon film, i.e., $x = -t_{\mathrm{si}/2}$ to 0, and substituting the boundary into it yields

$$\begin{aligned}\frac{(V_G - V_{\mathrm{FB}} - \phi_s)^2}{\gamma^2} &= \left[(\phi_s - \phi_b) + V_t \exp\left(\frac{-\phi_b}{V_t}\right) - V_t \exp\left(\frac{-\phi_s}{V_t}\right)\right] \\ &\quad + \left(\frac{n_i}{N_a}\right)^2\left[(\phi_b - \phi_s) + V_t \exp\left(\frac{\phi_s}{V_t}\right) - V_t \exp\left(\frac{\phi_b}{V_t}\right)\right],\end{aligned} \tag{10}$$

where $\gamma = \sqrt{2q\varepsilon_{\mathrm{si}}N_a}/C_{\mathrm{ox}}$ and $\phi_f = V_t \ln(N_a/n_i)$. To solve ϕ_s, another expression relating ϕ_s and ϕ_b is required. The relation is obtained from the condition of full depletion for body charge and the simplification of discretization of Eq. (3) [6–8]. According to the condition of full depletion for body charge $Q_b = C_{\mathrm{ox}}\gamma\sqrt{\phi_s - \phi_b} \le qN_a t_{\mathrm{si}}/2$, ϕ_b is given as $\phi_s - \lambda t_{\mathrm{si}} C_{\mathrm{ox}}(V_G - V_{\mathrm{FB}} - \phi_s)/2\varepsilon_{\mathrm{si}} - V_{\mathrm{xd}}$, where λ is a fitting parameter and $V_{\mathrm{xd}} = qN_a t_{\mathrm{si}}^2/8\varepsilon_{\mathrm{si}}$. The critical voltage $V_G = V_C$ at which is changed from partially depleted (PD) to the fully depleted (FD) device needs to be calculated before deriving the analytical solution. It will be derived from the condition that $\phi_b = 0$ and $\phi_s \approx V_{\mathrm{xd}}$.

$$V_C = V_{\mathrm{FB}} + V_{\mathrm{xd}} + \gamma\left\{V_{\mathrm{xd}} + V_t\left[\exp\left(\frac{-V_{\mathrm{xd}}}{V_t}\right) - 1\right] + V_t\left[\exp\left(\frac{V_{\mathrm{xd}} - 2\phi_f}{V_t}\right) - \exp\left(\frac{-2\phi_f}{V_t}\right)\right]\right\}^{1/2}. \tag{11}$$

Also, the analytical solution of surface potential is discussed in the (a) depletion and weak inversion and (b) strong inversion regions.

Firstly, surface potential of PD devices is discussed, i.e., $\phi_b = 0$. For the case of the depletion and weak inversion, Eq. (10) can be approximated and solved as

$$\phi_{\mathrm{sd}}^p = V_G - V_{\mathrm{FB}} + \gamma^2/2 - \gamma\sqrt{\gamma^2/4 + V_G - V_{\mathrm{FB}} + A}, \tag{12}$$

where $A = V_t\left(1 + \exp\left(-2\phi_f/V_t\right)\right)$ and ϕ_{sd}^p is the surface potential of a PD device in the depletion and weak inversion region. According to the studies [7,8], surface potential of the strong inversion region is given by

$$\phi_{\mathrm{si}}^p = f_\phi + V_t \ln\left\{\left[\left(V_G - V_{\mathrm{FB}} - f_\phi\right)^2/\gamma^2 - f_\phi + 1\right]\Big/ V_t\right\}, \tag{13}$$

where ϕ_{si}^p is the surface potential of a PD device in the strong inversion region. f_ϕ is empirically given as $f_\phi = (2\phi_f + \phi_{\mathrm{sd}}^p - \sqrt{(\phi_{\mathrm{sd}}^p - 2\phi_f)^2 + 4\delta^2})/2$ and δ is a calibrating parameter. As mentioned above, the surface

potential equation can be linked by the following smooth function [3,4], which is given as

$$\phi_{st}^{p} = \phi_{si}^{p} - V_t \ln\left\{1 + \exp\left[(\phi_{si}^{p} - \phi_{sd}^{p})/V_t\right]\right\}, \quad (14)$$

where ϕ_{st}^{p} is the surface potential of a partially depleted DG-MOSFET in all operating regions.

Next, surface potential of a fully depleted device is derived. For the case of the depletion and weak inversion, Eq. (10) can be approximated and solved as

$$\phi_{sd}^{f} = V_G - V_{FB} - \gamma\sqrt{V_{xd}}, \quad (15)$$

where ϕ_{sd}^{f} is the surface potential of a FD device in the depletion and weak inversion region. For the case of the strong inversion, the surface potential is given as

$$\phi_{si}^{f} = 2\phi_f + V_t \ln\{[(V_G - V_{FB} - f_\phi)^2/\gamma^2 - V_{xd}]/V_t[1 - \exp(-V_{xd}/V_t)]\}, \quad (16)$$

where ϕ_{si}^{f} is the surface potential of a FD device in the strong inversion region. Also, the surface potential equation can be linked by the following smooth function, which is given as

$$\phi_{st}^{f} = \phi_{si}^{f} - V_t \ln\left\{1 + \exp\left[(\phi_{si}^{f} - \phi_{sd}^{f})/V_t\right]\right\}, \quad (17)$$

where ϕ_{st}^{f} is the surface potential of a fully depleted DG-MOSFET in all operating regions. If a device can change the operation mode from PD device to FD device as V_G is increased, then the smooth function is employed to link the operation mode [4]:

$$\phi_s^m = \frac{\phi_{st}^{p}}{1 + l_1 \exp\left[(V_G - V_C)/n_1 V_t\right]} + \frac{\phi_{st}^{f}}{1 + l_1 \exp\left[-(V_G - V_C)/n_1 V_t\right]}, \quad (18)$$

where l_1 and n_1 are fitting parameters and ϕ_s^m is the unified surface potential.

3. Computational calibration and numerical results

3.1. Computational calibration

Since the solution is derived under the simplified assumption based on different operating regions, the error between the exact solution and the analytical solution should be subject to further minimization. Therefore, an adjustment term and fitting parameters are considered after deriving the solution of the Poisson equation and the explicit function of surface potential. By comparing Eq. (4) with Eqs. (5) and (8), we know that the slope of Eq. (4) is larger than or equal to the slope of Eqs. (5) and (8) for $x > 0$. The slope of Eq. (4) is smaller than or equal to the slope of Eqs. (5) and (8) for $x < 0$. An adjustment function is introduced to reduce the solution error. According to our analyses, the adjustment function, $\widetilde{E}(x) = ax^8 + bx^2$, shows a good approximation. a and b are fitting parameters. Then, the modified analytical solution is

$$\widetilde{\phi}(x) = \phi(x) - \widetilde{E}(x). \quad (19)$$

3.2. Results and discussion

In this study, double-gate NMOSFETs with different gate oxide thickness ($t_{ox} = 2, 3$ and 4 nm), silicon film thickness ($t_{si} = 20, 30$ and 40 nm), and doping concentration ($N_a = 10^{16}, 10^{17}$ and 10^{18} cm^{-3}) are simulated for different gate applied bias ($V_G = 0.1, 0.2, 0.4, 0.6, 0.8$ and 1.0 V). Under the given scenario, DG-MOSFETs will be fully depleted and surface potential is estimated by Eq. (16). From the results, the analytical solution of surface potential has an approximation with error, which is smaller than 0.005% in depletion and weak inversion region. In the strong inversion region, a larger error, which is smaller than 0.01%, is obtained. The results, which are given in Table 1, show that the explicit function gives good approximations of surface potential. Because the potential distribution varies widely, the approximated error in the strong inversion region is larger than the approximated error

Table 1
Numerical and analytical surface potentials of the simulated device

	Numerical (A)	Analytical (B)	Difference $(C) = \|(B) - (A)\|$	Error $(C)/(A)$ (%)
$V_G = 0.05$ V	0.940459	0.9405	0.000041	0.00436
$V_G = 0.1$ V	0.953597	0.953588	0.000009	0.00094
$V_G = 0.7$ V	1.03872	1.03866	0.00006	0.00578
$V_G = 1.0$ V	1.06509	1.06498	0.00011	0.010

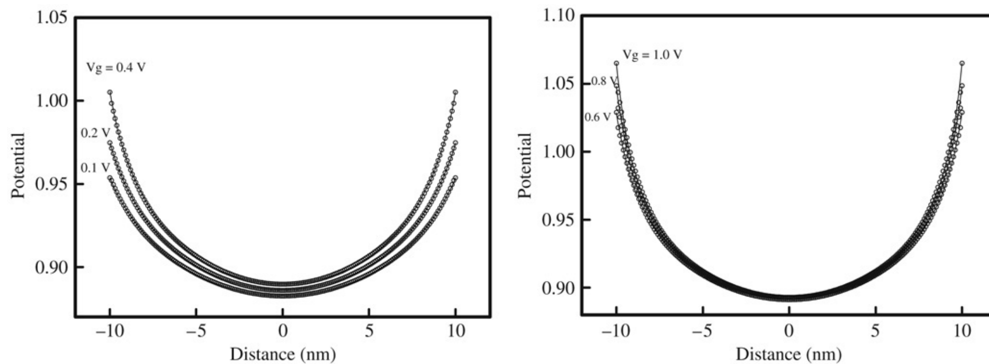

Fig. 3. Comparison of the numerical (solid lines) and analytical (symbols) potentials for the DG-MOSFET with respect to different V_G, where $t_{ox} = 2$ nm, $t_{si} = 20$ nm and $N_a = 10^{17}$ cm^{-3}.

Table 2
Relationship among the fitting parameters, N_a, t_{ox}, t_{si} and V_G

Parameter	N_a	t_{ox}	t_{si}	V_G
a	$\propto 1/N_a$	$\propto 1/t_{ox}$	$\propto t_{si}$	$\propto V_G$
b	$\propto N_a$	$\propto 1/t_{ox}$	$\propto 1/t_{si}$	$\propto V_G$

in the depletion and weak inversion region. The differentiation of the analytical solution of surface potential is smaller than the actual distribution. With the explicit surface potential, potential distributions are simulated and compared with numerical approximations, which are simulated by an iterative algorithm. The numerical program is calibrated by the measured data and considered as exact. Figs. 3–6 illustrate the comparison of numerical and analytical results. Different profiles of devices are compared to show the accuracy of the analytical solution presented in this work.

Fig. 3 examines the simulated results of DG-MOSFET ($t_{ox} = 2$ nm, $t_{si} = 20$ nm, and $N_a = 10^{17}$ cm^{-3}) under different gate applied bias ($V_G = 0.1, 0.2, 0.4, 0.6, 0.8$ and 1.0 V). It shows that the analytical results are in good agreement with the numerical results. The maximal error is about 0.7% and the average error is about 0.4%. Thus, the analytical solution is accurate enough to apply to circuit simulation. Fig. 4 illustrates the application of the analytical solution to simulate devices with different oxide thickness for $t_{si} = 20$ nm and $N_a = 10^{17}$ cm^{-3}. The error between the analytical and numerical solution is within 2%. Potential of DG-MOSFETs with different silicon thickness is simulated for $t_{ox} = 2$ nm and $N_a = 10^{17}$ cm^{-3} numerically and analytically in Fig. 5. We have found that the error fluctuations are all less than 4%. Fig. 6 illustrates the simulated results of DG-MOSFET with different doping concentration for $t_{si} = 20$ nm and $t_{ox} = 2$ nm. The error is within 2%. The relation between parameters and doping concentration, oxide thickness, channel thickness and gate voltage are given in Table 2. From the figures, the error increases at the top and bottom surface with the gate bias.

According to the results, the approximations of the analytical solution also present good agreement with the numerical results. The maximal error is about 4% and the average error is about 1%. If we go a step further to examine the simulated data, the maximal error always occurs near the surface of the channel in all cases. From Eq. (4), the first derivative of potential varies largely near the surface of the channel. However, the approximation, which is determined

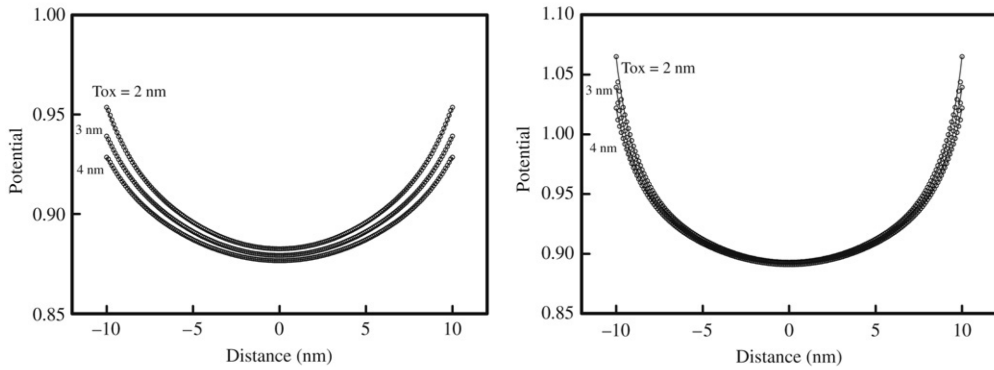

Fig. 4. Comparison of the numerical and analytical potentials for the DG-MOSFET with respect to different t_{ox}, where $t_{\mathrm{si}} = 20$ nm and $N_a = 10^{17}\ \mathrm{cm}^{-3}$. The left figure is with $V_G = 0.1$ V and the right one is with $V_G = 1.0$ V.

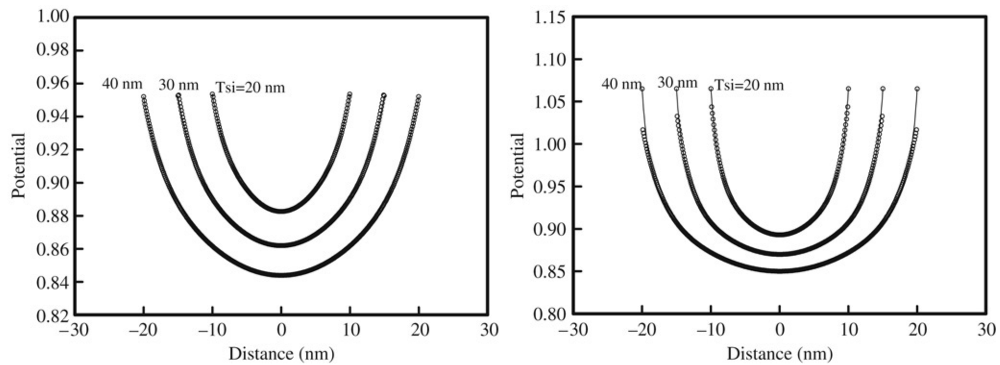

Fig. 5. Comparison of the numerical and analytical potentials for the DG-MOSFET with respect to different t_{si}, where $t_{\mathrm{ox}} = 2$ nm and $N_a = 10^{17}\ \mathrm{cm}^{-3}$. The left figure is with $V_G = 0.1$ V and the right one is with $V_G = 1.0$ V.

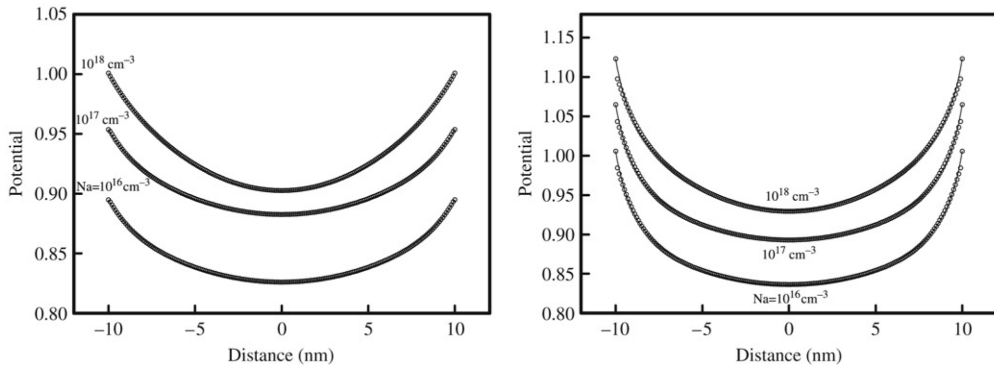

Fig. 6. Comparison of the numerical and analytical potentials for the DG-MOSFET with respect to different N_a, where $t_{\mathrm{si}} = 20$ nm and $t_{\mathrm{ox}} = 2$ nm. The left figure is with $V_G = 0.1$ V and the right one is with $V_G = 1.0$ V.

by Eqs. (5) and (8), is smaller than that. Fortunately, the error is small enough to be neglected without influencing the accuracy of circuit simulation and estimating electron density. In addition, the solution is accurate enough to describe the potential distribution of nanoscale DG-MOSFETs. It can be a helpful equation while simulating the characteristics of DG-MOSFETs so as to design advanced devices.

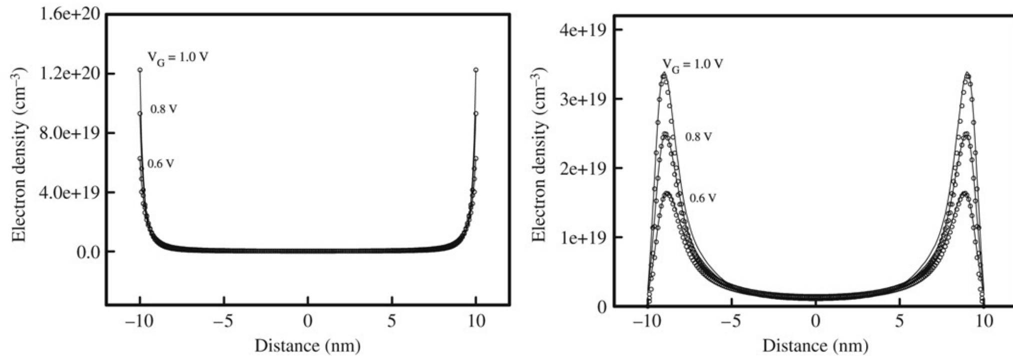

Fig. 7. The classical (left figure) and quantum corrected (right figure) electron densities using the derived potential solution. Comparison of the numerical and analytical results for the DG-MOSFET with respect to different V_G, where $N_a = 10^{17}$ cm^{-3}, $t_{\text{ox}} = 2$ nm and $t_{\text{si}} = 20$ nm.

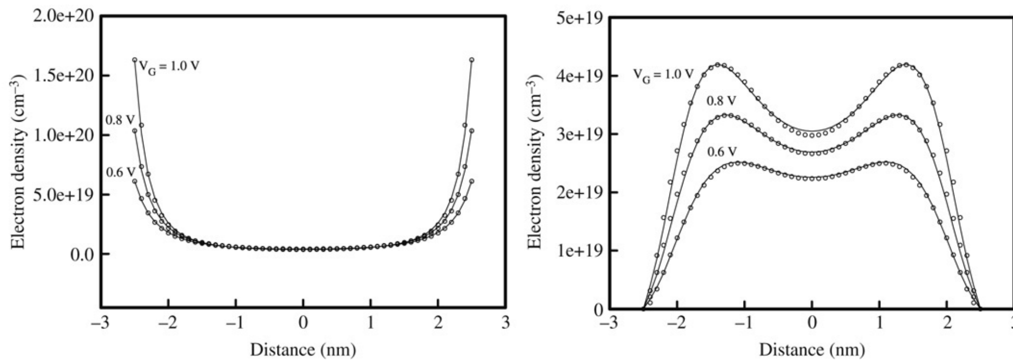

Fig. 8. The classical (left figure) and quantum corrected (right figure) electron density using the derived potential solution. Comparison of the numerical and analytical results for the DG-MOSFET with respect to different V_G, where $N_a = 10^{17}$ cm^{-3}, $t_{\text{ox}} = 2$ nm and $t_{\text{si}} = 5$ nm.

4. Application to quantum correction of electron density

As mentioned above, the analytical solution presents accurate results and time-efficient solving methods for the potential of DG-MOSFETs. Since classical potential of a device is obtained, with Boltzmann statistics electron density can be calculated by the following formula

$$n_{\text{CL}} = n_i \exp\left(q\left(\phi - \phi_n\right)/kT\right). \quad (20)$$

In Eq. (20), n_{CL} is classical electron density, ϕ_n is quasi-Fermi potential of electron and k is Boltzmann's constant. Furthermore, the electron density with quantum effect is obtained by coupling the quantum correction model [9–13] with the classical electron density. The unified quantum correction model is given as

$$n_{\text{QM}} = a_0 n_{\text{CL}} \left[1 - \exp\left(-a_1 \xi^2 \left(1 - \frac{1}{2}\left(\frac{\xi}{\xi_0}\right)^2\right) - a_2 \xi^3\right)\right], \quad (21)$$

where n_{QM} is quantum electron density, a_0, a_1 and a_2 are fitting parameters, $\xi_0 = T_{\text{si}}/2\lambda_{\text{th}}$, $\xi = x/\lambda_{\text{th}}$ and $\lambda_{\text{th}} = \left(\hbar/2 \times 9.11 \times 10^{-31} kT\right)$. $\hbar$ is the reduced Planck constant. Classical and quantum electron density of a DG-MOSFET with $t_{\text{ox}} = 2$ nm, $t_{\text{si}} = 20$ nm and $N_a = 10^{17}$ cm^{-3} are shown in Fig. 7. Examining the application of the analytical solution to nanoscale devices, we simulate a $t_{\text{si}} = 5$ nm, $t_{\text{ox}} = 2$ nm, $N_a = 10^{17}$ cm^{-3} DG-MOSFET. Fig. 8 shows the classical and quantum electron density. The analytical results show good agreement with the numerical results [9–13]. Therefore, the analytical solution of the Poisson equation provides a way to simulate nanoscale DG-MOSFET.

5. Conclusions

In this study, a 1-D analytical solution of the Poisson equation for symmetric DG-MOSFET is derived successfully. The solution works for PD and FD DG-MOSFET devices with different doping concentration. According to the numerical comparison, the results are accurate under different applied gate bias and device parameters. The error is within 4% in all simulated scenarios. We note that the analytical solution can be incorporated into a quantum correction model for the numerical simulation of nanoscale DG-MOSFETs. We are currently deriving the solution for the case of asymmetric DG-MOSFETs.

Acknowledgments

This work was supported in part by the National Science Council of TAIWAN under Contract NSC-95-2221-E-009-336, Contract NSC-95-2752-E-009-003-PAE, Contract NSC-96-2415-H-216-001, by the MoE ATU Program, Taiwan under a 2006–2007 grant, and by the Taiwan semiconductor manufacturing company under a 2006–2007 grant.

References

[1] Y. Li, H.-M. Chou, A comparative study of electrical characteristic on sub-10-nm double-gate MOSFETs, IEEE Transactions on Nanotechnology 4 (2005) 645–647.
[2] Y. Li, S.-M. Yu, A two-dimensional quantum transport simulation of nanoscale double-gate MOSFETs using parallel adaptive technique, IEICE Transactions on Information and Systems E87-D (2004) 1751–1758.
[3] A. Rahman, M.S. Lundstrom, A compact scattering model for the nanoscale double-gate MOSFET, IEEE Transactions on Electron Devices 49 (2002) 481–489.
[4] Y. Taur, Analytical solutions of charge and capacitance in symmetric and asymmetric double-gate MOSFETs, IEEE Transactions on Electron Devices 48 (2001) 2861–2869.
[5] S. Xiong, J. Bokor, Sensitivity of double-gate and FinFET devices to process variations, IEEE Transactions on Electron Devices 50 (2003) 2255–2260.
[6] S.-L. Jang, B.-R. Huang, J.-J. Ju, A unified analytical fully depleted and partially depleted SOI MOSFET model, IEEE Transactions on Electron Devices 46 (1999) 1872–1876.
[7] R. van Langevelde, F.M. Klaassen, An explicit surface-potential-based MOSFET model for circuit simulation, Solid-State Electronics 44 (2000) 409–418.
[8] Y.S. Yu, S.W. Hwang, D. Ahn, A unified analytical SOI MOSFET model for fully- and partially-depleted SOI devices, in : Proc. Asia-Pacific Workshop on Fundamental and Application of Advanced Semiconductor Devices, 4–7 July, 2001, pp. 329–334.
[9] Y. Li, S.-M. Yu, A unified quantum correction model for nanoscale single- and double-gate MOSFETs under inversion condition, Nanotechnology 15 (2004) 1009–1016.
[10] Y. Li, A comparison of quantum correction models for nanoscale MOS structures under inversion conditions, Materials Science Forum 480–481 (2005) 603–610.
[11] Y. Li, A quantum correction Poisson equation for metal-oxide-semiconductor structure simulation, Semiconductor Science and Technology 19 (2004) 917–922.
[12] Y. Li, T.-W. Tang, S.-M. Yu, A quantum correction model for nanoscale double-gate MOS devices under inversion conditions, Journal of Computational Electronics 2 (2003) 491–495.
[13] T.-W. Tang, Y. Li, A SPICE-compatible model for nanoscale MOSFET capacitor simulation under the inversion condition, IEEE Transactions on Nanotechnology 1 (2002) 243–246.